SSRG International Journal of Recent Engineering Science
ISSN: 2349–7157 / https://doi.org/10.14445/23497157/IJRES-V11I4P111

Volume 11 Issue 4, 81-92, Jul-Aug 2024

Original Article

Efficient Power Management System of PV, Fuel Cell and Bess-Based DC Microgrid System

E. Kalaiyarasan[1], S. Singaravelu[2]

[1,2]*Electrical Engineering, Annamalai University, Tamilnadu, India.*

[1]*Corresponding Author : kalaiyarasan.a.m@gmail.com*

Received: 29 May 2024 Revised: 06 July 2024 Accepted: 25 July 2024 Published: 14 August 2024

Abstract *- This study explores a state-of-the-art power management system for a DC microgrid, integrating a 1 kW, 120 V Photovoltaic (PV) system and a Proton Exchange Membrane Fuel Cell (PEMFC), both employing Adaptive Neuro-Fuzzy Inference System (ANFIS) Maximum Power Point Tracking (MPPT) controllers. The PV system, with a 220 V output, utilizes a Switched Inductor DC-DC (SIDC) converter, which optimizes the energy conversion. Simultaneously, the PEMFC delivered 1.26 kW at 220 V by integrating ANFIS MPPT control and a SIDC converter for heightened efficiency. The Battery Energy Storage System (BESS) incorporates a bidirectional converter with a Proportional-Integral (PI) controller, facilitating optimal bidirectional power flow for efficient charging and discharging operations. Central to the microgrid is a DC bus architecture that promotes seamless integration among PV, PEMFC and BESS components. The DC load ranges from 500 to 700W and has been integrated with the DC bus. This robust Power Management System, including protective mechanisms, ensures the microgrid's stability and reliability. The power Management System incorporates predictive analytics by orchestrating the dynamic operation of PV, PEMFC and BESS components to meet fluctuating energy demand. The power management across the DC micro-grid is studied by three different scenarios based on demand-side management. This work contributes to the evolving landscape of microgrid technology, aligning with current trends in sustainable energy solutions. The detailed exploration of specific components, including ANFIS MPPT controllers, SIDC converters and bidirectional BESS control, provides valuable insights into the technical intricacies and challenges associated with this integrated approach.*

Keywords *- Energy, ANFIS, Microgrid, Photovoltaics, BESS, Green energy.*

1. Introduction

In the persistent search for sustainable and efficient energy solutions, the integration of diverse technologies in microgrid systems has emerged as a focal point for researchers and engineers alike. This study explores an innovative energy management system designed for a DC microgrid, where the convergence of PV panels [1], PEMFC [2] and a BESS [3] promises to redefine the landscape of decentralized power distribution. Through intricate control strategies and advanced converter technologies, this integrated approach seeks to address the challenges of optimizing energy production, storage, and distribution in a harmonized manner.

The urgency of transitioning toward cleaner and more resilient energy systems is underscored by the escalating global energy demand, coupled with the imperative to mitigate the environmental impacts of traditional power generation. In this context, the proposed DC microgrid [4] stands as a testament to the potential inherent in combining renewable energy sources with cutting-edge energy storage and management systems. The strategic integration of a 1 kW, 120 V PV system, a PEMFC delivering 1.28 kW at 220 V and a BESS equipped with bidirectional converters [5] adds layers of complexity and opportunity to the microgrid paradigm.

The PV system serves as the cornerstone of the microgrid, converting sunlight into electrical energy through photovoltaic cells. The system's 1 kW capacity, coupled with a 120 V rating, positions it as a formidable contributor to the overall energy matrix. To extract maximum power from the PV panels, an ANFIS[6] MPPT controller has been implemented. This controller, with its adaptive learning capabilities, ensures that the PV system operates at its peak efficiency under varying environmental conditions. Complementing the PV system is the PEMFC, a dynamic source of continuous power generated through electrochemical reactions. Delivering 1.28 kW at 220 V, the PEMFC becomes a critical component in the microgrid, particularly during periods of reduced solar irradiance. Employing an ANFIS MPPT controller, the fuel cell is seamlessly integrated into the microgrid, and its power output is optimized to synchronize with the overall energy demand. The BESS acts as the reservoir of the microgrid, providing a means to store excess energy generated by the PV system and

PEMFC during peak production periods. The BESS is equipped with bidirectional converters, which facilitate efficient charging and discharging operations. A PI controller governs the bidirectional converter, ensuring precise and responsive control over the energy flow in and out of the storage system. This dynamic control capability becomes crucial in adapting to the fluctuations in energy demand and supply by contributing to the overall stability and reliability of the microgrid.

The pivotal point of interaction among these diverse energy sources and storage elements is the DC bus architecture. The DC bus acts as the central hub, facilitating the interconnection of the PV system, PEMFC and BESS. Its role in coordinating and managing the flow of energy within the microgrid is indispensable, laying the foundation for a seamlessly integrated and highly responsive system. The microgrid's reliability and stability are further fortified by a robust Power Management System (PMS) [7], incorporating protective mechanisms to safeguard against potential disturbances or faults. The PMS ensures that the microgrid operates within safe and efficient limits, contributing to the resilience of the overall energy distribution system. Integral to this is the implementation of SIDC converters for both the PV system and PEMFC. These converters play a crucial role in transforming and regulating the DC output voltages to match the requirements of the microgrid, which enhances the compatibility and efficiency of the entire system.

At the core of this sophisticated microgrid is the Power Management System, orchestrating the dynamic interplay of the PV system, PEMFC and BESS. The EMS, leveraging predictive analytics and real-time monitoring, optimizes the operation of each component in response to changing energy demand patterns. Its adaptive control strategies, rooted in advanced technologies such as Adaptive Neuro-Fuzzy Inference Systems and intelligent algorithms [8], position the microgrid as a smart and responsive energy distribution system [9]. Efficiency optimization strategies embedded in the EMS encompass demand-side management [10] and economic considerations.

Beyond the technical intricacies, the proposed microgrid addresses critical environmental concerns by reducing carbon footprints [11]. A comprehensive life cycle analysis evaluates the sustainability of the entire system, taking into account the environmental impacts from manufacturing to end-of-life. This holistic approach aligns with the evolving trends in sustainable energy solutions, acknowledging the need for not just efficient but also environmentally responsible energy systems. The integration of PV, PEMFC and BESS within a DC microgrid, coupled with an advanced Energy Management System, presents a transformative solution for efficient, reliable and sustainable energy distribution [12]. The overall block diagram of the proposed work is shown in Figure 1.

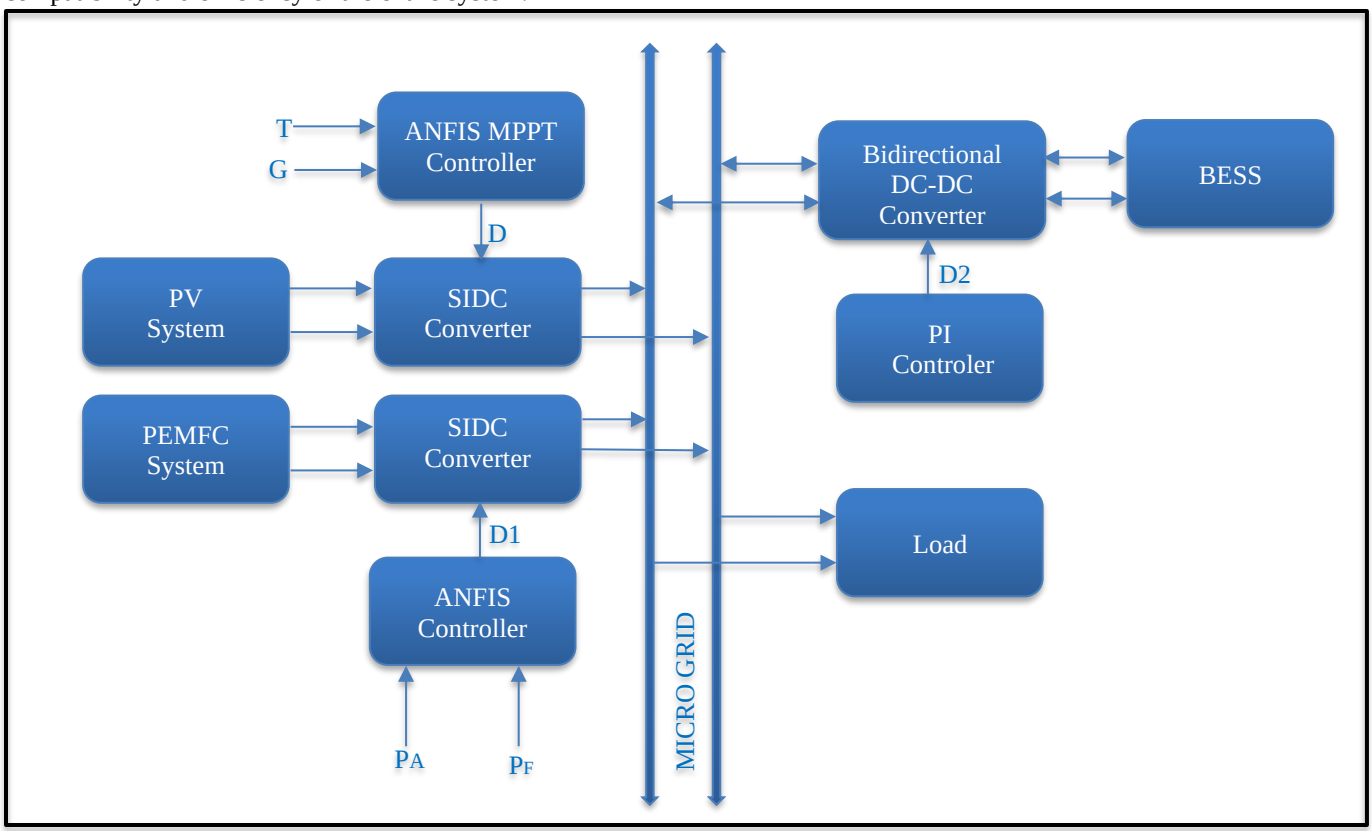

Fig. 1 Overall block diagram of the proposed work

This study delves into the technical nuances, challenges and potential applications of this integrated approach, which provides a comprehensive understanding of the evolving landscape of microgrid technology [13]. The intricate balance achieved through the synergies of diverse energy sources, advanced control strategies and responsive energy management positions this microgrid as a model for future decentralized power distribution systems. As the world navigates towards a more sustainable energy future, the insights from this research contribute to the ongoing discourse on resilient and environmentally conscious energy systems.

The methodology of the proposed work has been partitioned as follows: Section two deals with the description of PV system parameters, the design of the PEMFC system and the rating of the battery energy storage system. Section three explores the design of SIDC for both PV and PEMFC, the design of a bi-directional DC-DC converter for BESS and Section four deals with the optimization of the ANFIS model for MPPT control of both PV and PEMFC system and PI controller for BESS. Section five interprets the performance analysis of the overall integration of PV, PEMFC and BESS systems for efficient energy management strategy in a DC microgrid using smart controllers.

2. Depiction of System Parameters

In this section, the work explores the intricate details of system parameters and design considerations for three critical components of renewable energy systems such as photovoltaic systems, PEMFC systems and BESS. Each of these components plays a vital role in harnessing, storing and utilizing renewable energy efficiently and sustainably.

2.1. Description of Pv System Parameters

A PV array represents the heart of any photovoltaic installation, serving as the primary source of electrical power. It is comprised of individual solar panels, each equipped with semiconductor materials that convert solar radiation into Direct Current (DC) electricity. The collective arrangement of these panels in a PV array forms a robust and scalable energy generation platform. The single diode equivalent circuit represents a PV cell/module as an electrical circuit consisting of a current source, a diode, a series resistor (R_s), and a shunt resistor (R_{sh}) connected in parallel with the diode, as shown in Figure 2.

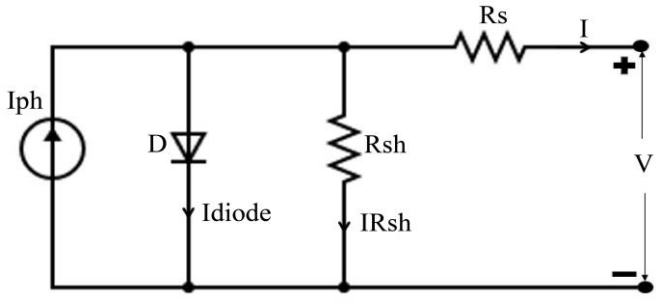

Fig. 2 Electrical equivalent circuit of the solar array

2.1.1. Current-Photovoltaic Current (I_{ph})

The photovoltaic current (I_{ph}) is the current generated by the PV cell/module due to sunlight. It is determined by the intensity of solar irradiance (G) and the cell/module's area (A_{cell}), as shown in Equation 1.

$$I_{ph} = G \times A_{cell} \times I_{sc} \quad [1]$$

Where:
I_{SC} is the short-circuit current of the cell/module.

2.1.2. Current-Diode Current (I_{diode})

The diode current (I_{diode}) represents the current passing through the diode. It depends on the cell/module's voltage (V), the diode ideality factor (n), the diode reverse saturation current (I_0), and the thermal voltage (V_T) as given in Equation 2.

$$I_{diode} = I_O(\exp \exp \left(\frac{qV}{nkT}\right) - 1) \quad [2]$$

Where:
q is the charge of an electron, k is Boltzmann's constant, and T is the absolute temperature in Kelvin.

2.1.3. Current-Series Resistance (I_{Rs})

The series resistance (R_s) represents the resistance in series with the diode. It affects the overall performance and reduces the maximum power output. It can be determined from the voltage drop across it (V_{Rs}) and the current (I), as shown in Equation 3.

$$V_{Rs} = I * R_s \quad [3]$$

2.1.4. Current-Shunt Resistance (I_{Rsh})

The shunt resistance (R_{sh}) represents the resistance in parallel with the diode. It is very high in good PV modules, and thus, it does not significantly affect the performance. The total current (I) in the circuit is the sum of the photovoltaic current, diode current, and the series resistance current, as given in Equation 4.

Table 1. PV array specifications

Parameters	Values
Open circuit voltage/cell	0.74V
Maximum voltage/cell	0.66V
Number of cells	60
Open circuit voltage /module	37.1V
Short circuit current/module	8.92A
Maximum voltage /module	29.9V
Maximum current/module	8.35A
Number of parallel strings	1
Number of series strings	4
Array Open circuit voltage	148.4V
Array Short circuit current	8.92A
Array Maximum voltage	119.6V
Array Maximum current	8.35A
Array Maximum power	998.66W

$$\text{The total current (I)} = I_{ph} - I_{diode} - \frac{V}{R_s} + \frac{V}{R_{sh}} \quad [4]$$

Power output is calculated as the product of voltage and current as given in Equation 5

$$P = I * V \quad [5]$$

In this study, the most reliable monocrystalline silicon (m-Si) solar cell-based 1KW PV array is constructed in the MATLAB/SIMULINK platform. The technical specifications of one kilowatt PV array are given in Table 1.

2.2. Design of the PEMFC System

The operational temperature significantly impacts the performance of a fuel cell with a deviation affecting both efficiency and power generation. Excessive heat can lead to decreased efficiency and power output while operating at higher temperatures can enhance the utilization of residual heat. Optimal temperature management is crucial to operate fuel cells most effectively within a specific temperature range. Achieving and maintaining this ideal temperature is supreme for ensuring the fuel cell's reliability and optimal performance. In the search for sustainable and efficient energy solutions, PEMFCs have emerged as a cutting-edge technology by utilizing the chemical energy of hydrogen to generate electricity with remarkable efficiency and minimal environmental impact. Substantial research efforts have been dedicated to advancing PEMFC technology, especially over the last few decades, contributing to its evolution as a promising and impactful solution in the field of clean energy [14]. The schematic diagram of the PEM fuel cell is shown in Figure 3.

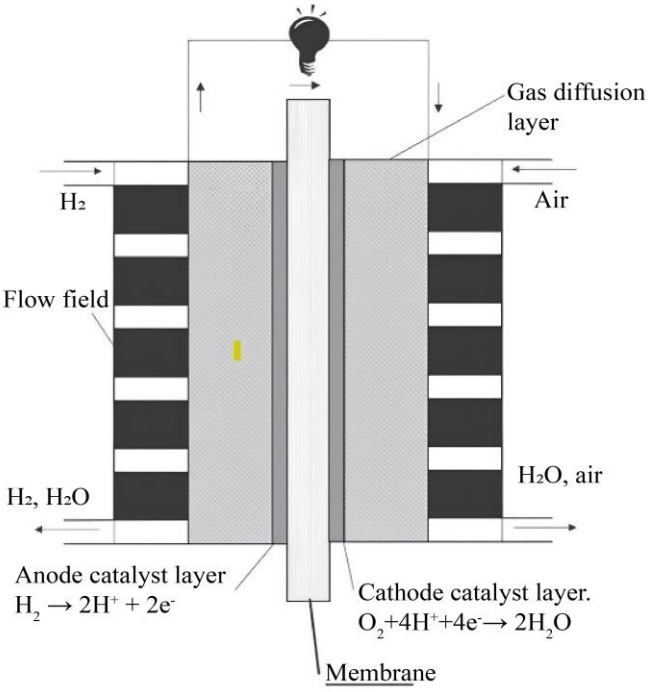

Fig. 3 Schematic diagram of PEM fuel cell [15].

In a PEMFC, the polymer-electrolyte membrane plays a central role by facilitating ion conduction while impeding electron transfer between electrodes. The catalyst layers within the membrane house intricate structures composed of precious metal nanoparticles supported on porous carbon and ionomer, establishing pathways for the transport of reactants, products, electrons and protons to and from active sites where electrochemical reactions take place.

The anode is responsible for fuel oxidation when hydrogen is utilized to release protons and electrons. Protons move through the membrane while electrons navigate the external circuit [15]. At the cathode catalyst layer, protons and electrons recombine with oxygen, which results in the production of water. The membrane and electrodes are enclosed between graphite blocks featuring gas flow channels and porous diffusion media to ensure the distribution of gaseous hydrogen and oxygen across electrodes and the completion of the electron flow circuit. These carbon media include a macro-porous gas-diffusion layer and a microporous layer adjacent to the catalyst layer contributing to the efficient functioning of the PEMFC [15].

The stack power (P_{stack}) can be calculated by considering the voltage (V_{cell}) across a single cell and the current (I_{stack}) passing through the stack in the account of a number of cells (N_{cells}) in the stack. Ohm's Law gives the relationship:

$$P_{stack} = I_{stack} \times V_{cell} \times N_{cells} \quad [6]$$

The voltage across a single PEMFC (V_{cell}) is a function of the actual cell potential (E_{cell}), the current passing through the stack (I_{stack}) and the internal resistance of the cell (R_{int}). This relationship can be expressed as follows:

$$V_{cell} = E_{cell} - I_{stack} \times R_{int} \quad [7]$$

$$E_{cell} = E^{o}_{cell} - \frac{RT}{nF} \ln\left(\frac{P_{O2}}{\sqrt{P_{H2}}}\right) \quad [8]$$

$$I_{stack} = \frac{V_{stack}}{R_{int}+R_{ext}} \quad [9]$$

Where, E^{o}_{cell} is the standard cell potential, R is the ideal gas constant, T is system temperature, n is the number of electrons involved in the reaction (n=2 in this case), R_{ext} is the external resistance in the fuel cell circuit, F is Faraday's constant, P_{O2} and P_{H2} are the partial pressures of air and water vapor respectively.

The reference parameters of the PEMFC stack have been extracted from SIMULINK with 24V and 1.26KW PEMFC, as given in Table 2. The electrical characteristics of the PEMFC Stack with nominal and maximum values of stack voltage, current and power are shown in Figure 4.

Table 2. Description of PEMFC stack

S. No	Parameter	Value
1	Standard Cell Potential (E^{o}_{cell})	1.115V
2	Ideal gas constant (R)	8.314 J/(mol·K)
3	System temperature (T)	328K
4	Faraday's constant (F)	96,485 C/mol
5	Nominal utilization of H2 (P_{H2})	99.92%
6	Nominal utilization of O2 (P_{O2})	1.813%
7	I_{stack} nominal	52A
8	I_{stack} maximum	100A
9	V_{stack} nominal	24.23V
10	V_{stack} maximum	20V
11	P_{stack} nominal	1259.96W
12	P_{stack} maximum	2000W
13	R_{int}	0.061871 Ω

$$\eta(\%) = \frac{P_{OUT}}{P_{IN}} \times 100 \quad [10]$$

Where P_{OUT} is the electrical power output, and P_{IN} is the fuel input power.

P_{IN} is calculated by multiplying the nominal consumption of fuel with the Lower Heating Value (LHV) of hydrogen. The efficiency (η) of the system can then be determined by comparing the useful work output to the input energy:

$$P_{IN} = Q_{IN} = \text{Nominal fuel consumption} \times \text{LHV of hydrogen} \quad [11]$$

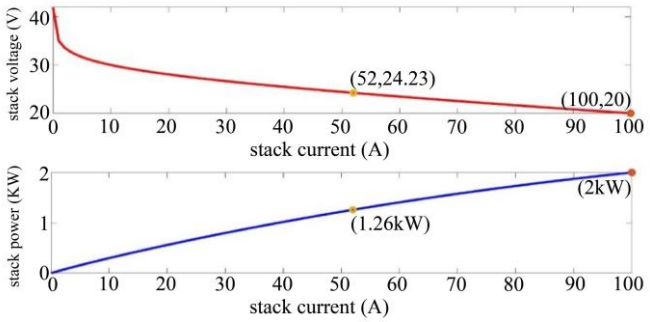

Fig. 4 Electrical characteristics of PEMFC Stack

2.3. Rating of Battery Energy Storage System

The suitability of a battery for a renewable energy system depends on various factors, which include the specific requirements of the system, the available technology and budget considerations. The most commonly used battery storage technologies are Lead-acid and Lithium-ion batteries. Lead-acid batteries are one of the most established and cost-effective options for renewable energy systems. They are suitable for off-grid backup power applications, but they have limitations in terms of cycle life and energy density. Lithium batteries come in various chemistries like lithium-ion (Li-ion) and lithium polymer (LiPo) batteries, with a nominal voltage of 3.7 volts per cell [16]. Lithium-ion batteries have gained popularity in recent years due to their high energy density, longer cycle life and faster charge and discharge capabilities.

The nominal current discharge characteristics curve of a lithium-ion battery covers more nominal area than that of a lead-acid battery, implying that the lithium-ion battery offers a higher energy density and potentially better performance in terms of capacity and power output, as shown in Figure 5. A 24V, 150AH Li-ion battery has been implemented in this work in view of its advantages and suitability. The battery current (I_{bat}) for a 24V, 150Ah battery can be calculated using Ohm's Law, which states that current is equal to voltage divided by resistance. The relationship in the context of a battery (very low battery resistance) is shown in Equation 1,

$$I_{bat} = \frac{Q}{t} \quad [12]$$

Were:
Q is the charge (AH), and t is the time (hours).
In this case, the battery current is 150A (t = 1hour).

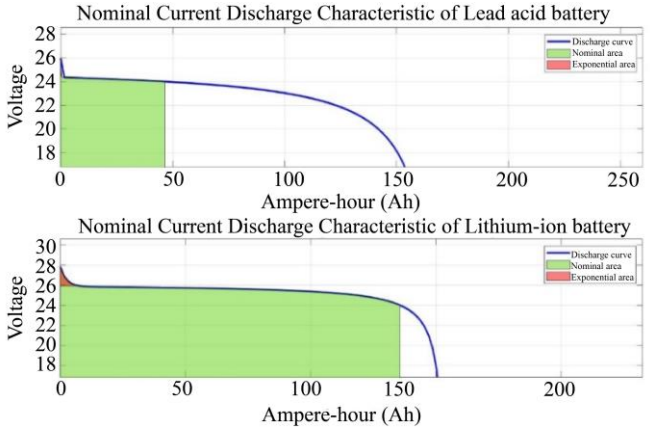

Fig. 5 Nominal current discharge characteristics of Li-ion and lead acid batteries

3. Design of Converters

3.1. Design of Bi-Directional DC-DC Converter for Bess

The bidirectional DC-DC buck-boost converter is at the heart of energy transfer within the projected system. Designing the converter elements, such as switches, inductors and capacitors, is the most critical step.

The converter is designed by taking into account efficiency, voltage regulation and response to fluctuations. The functional circuit diagram of the bi-directional DC-DC buck-boost converter is shown in Figure 6.

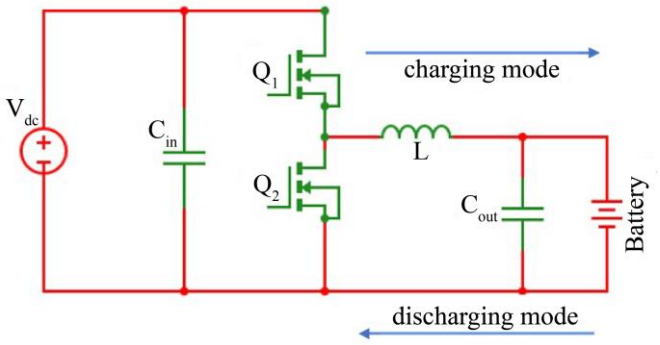

Fig. 6 Operating circuit of bidirectional DC-DC buck/boost converter

The duty cycle (D) is key for controlling the output voltage of the converter. The duty cycle less than 1 is for a buck converter (step-down), while it is greater than 1 for a boost converter (step-up). The duty cycle of dc-dc converter is calculated as given in Equation 13,

$$D = \frac{V_{bat}}{V_{in}} \quad [13]$$

The desired peak-to-peak inductor current ripple current is calculated by considering 20% of ripples in battery current, which is given in Equation 14,

$$\Delta I_L = 0.2 * I_{bat} \quad [14]$$

The value of inductor (L) is calculated by using the equation 15,

$$L = \frac{V_{in\_min}*(1-D)}{(f*\Delta I_L)} \quad [15]$$

Were,
V_{in_min} is V_{in} and f = 100KHZ.
The desired input voltage ripple is calculated using equation 16,

$$\Delta V_{L1} = 0.01 * V_{in} \quad [16]$$

The input filter capacitance and output capacitance are calculated by using Equations 17 and 19, respectively,

$$C_{IN} = \frac{(I_{bat}*D)}{(\Delta V_{L1}*f)} \quad [17]$$

The desired output voltage ripple is calculated using equation 18,

$$\Delta V_{L2} = 0.01 * V_{bat} \quad [18]$$

$$C_{OUT} = \frac{(I_{bat}*(1-D))}{(\Delta V_{L2}*f)} \quad [19]$$

The switching components are selected on the basis of the following criteria. The forward voltage drops across the diode (V_{f_diode} = 0.5). The maximum input voltage during boost mode is calculated as given in equation [20] by assuming the voltage stress (V_{ds_max}) on the switch is equal to V_{in_max},

Table 3. Bidirectional DC-DC buck-boost converter specifications

S. No	Parameters	Values
1	I_{bat}	150AH
2	Switching frequency	100KHZ
3	L	6.53333e-05 H
4	C_{IN}	7.43802e-05 F
5	C_{OUT}	5.56818e-03 F
6	V_{ds_switch}	272.13 V

$$V_{in\_max} = \frac{V_{in}}{(1-D)} \quad [20]$$

The safety margin for voltage stress on the switch ($V_{ds\_safe\_margin}$)= 0.1 * V_{in_max}.
The actual voltage stress on the switch is given in Equation 21,

$$V_{ds\_switch} = V_{in\_max} + V_{f\_diode} + V_{ds\_safe\_margin} \quad [21]$$

$$\text{Converter efficiency} = P_{out}/P_{in} \quad [22]$$

The calculations of the proposed bidirectional DC-DC buck-boost converter were done by using the equations mentioned above, which are listed in Table 3.

3.2. Design of SIDC Converter

The envisioned SIDC aims to address the specific challenges encountered by standalone PV systems, which grapple with fluctuations in solar irradiance and varying loads and the same methodology for PEMFC systems. The fundamental constituents of this converter comprise two inductors (L_1 and L_2), two switches (M_1 and M_2), the input voltage source (V_{in}), two input capacitors (C_1 and C_2), the output capacitor (C_{out}), seven diodes and the output load (R_L). Together, these components collaborate to facilitate effective power conversion and regulation. Figure 7 illustrates the simulation model of the SIDC converter.

During Mode 1, both switches M_1 and M_2 in the converter are in the ON state. Diodes D_1, D_2, and D_0 are forward-biased due to the polarity of the inductors and the input voltage source V_{in}. Inductors L_1 and L_2 are connected in parallel, allowing them to charge simultaneously. Energy is transferred to the inductors from the input voltage source, the energy stored in capacitor C_1 (VC_1), and the energy stored in capacitor C_2 (VC_2). This energy transfer results in an increase in the current flowing through the inductors. Since L_1 and L_2 are connected in parallel and have the same voltage source, which is denoted as VL_1 and VL_2, the load connected to the converter is powered by a combination of the input voltage, the Voltage across C_1 (VC_1), the Voltage across C2 (VC_2).

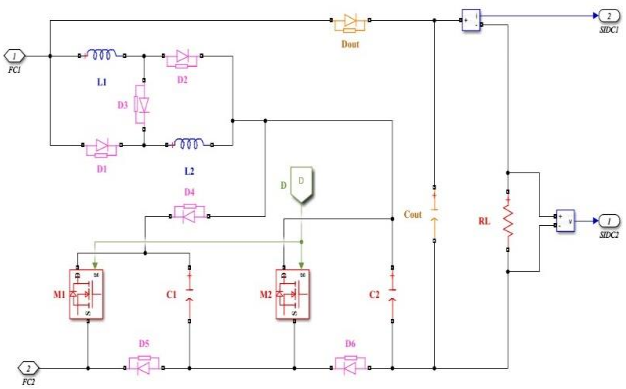

Fig. 7 Simulation diagram of SIDC converter

During Mode 2, both switches M_1 and M_2 in the converter are in the OFF state. As a result, the diodes D_1, D_2, and D_0 become reverse-biased and do not conduct current. In contrast, diodes D_3, D_4, D_5, and D_6 are forward-biased and allow current to flow through them. This voltage represents the energy stored in the inductors and is an important aspect of the converter's operation. In Mode 2, both inductors L_1 and L_2 are connected in series with each other. The series configuration causes them to cooperate in discharging their stored energy. The energy stored in the inductors is dissipated into capacitors C_1 and C_2 equally during this mode. Capacitors C_1 and C_2 act as energy storage devices and absorb the energy previously stored in the inductors. During this period, the load is supplied by the energy stored in the capacitor C_{out}. Capacitor C_{out} serves as the primary source of power to the load in Mode 2.

The average voltage of the SIDC converter when it is operated in a continuous mode of operation is calculated using reference [17] as given below,

$$\frac{V_{out}}{V_{PEMFC}} = \frac{3-D}{(1-3D)} = \text{voltage transfer ratio} \quad [23]$$

The R_L is calculated using the $P_{out,}$ and V_{out} is given as,

$$R_L = \frac{{V_{out}}^2}{P_{out}} \quad [24]$$

The voltage across the capacitor (C_1) can be calculated as,

$$VC_1 = \frac{1+D}{1-3D} = VC_2 \quad [25]$$

Switching frequency (f) of 100 kHz has been chosen. Now, the inductor and its current values can be calculated as given below in reference to [17],

$$L = \frac{V_{PEMFC}+VC_1}{\Delta I_L} * D * f = L_1 = L_2 \quad [26]$$

$$I_L = \frac{1}{1+D}\left(\frac{{V_{out}}^2}{V_{PEMFC}*R_L} - \frac{D*V_{out}}{R_L}\right) \quad [27]$$

The output capacitance (C_{out}) is determined by the desired voltage ripple (ΔV_{out} is calculated by considering 1% of V_{out}) and the load current (I_{out}). Let us consider a reasonable value for ΔV_{out} = 2.2V (1% of V_{out}),

$$I_{out} = \frac{P_{out}}{V_{out}} \quad [28]$$

$$C_1 = \left(\frac{2I_L+I_{out}}{\Delta VC_1}\right) D * f \quad [29]$$

$$C_2 = \left(\frac{I_{out}}{\Delta VC_2}\right) D * f \quad [30]$$

$$C_{out} = \frac{I_{out}*(1-D)}{\Delta V_{out}*f} \quad [31]$$

4. Design of Controllers

4.1. Modelling Of MPPT Controller for PV and PEMFC System

The MPPT controllers play a vital role in tracking the maximum power from the sunlight at all times during dynamic climatic conditions. The investigations are carried out to introduce efficient and reliable MPPT controllers.

Recent researches prove that the intervention of AI-based controllers effectively replaces the conventional MPPT controllers which are already in use. In this work, the optimized ANFIS MPPT controller has been developed and applied for both PV and PEMFC systems. The optimized model development is depicted below.

ANFIS is a hybrid computational model that combines elements of fuzzy logic and neural networks. It is primarily used for modeling complex, nonlinear relationships between input and output data. ANFIS is a type of fuzzy inference system that adjusts its parameters through a learning process, making it capable of adapting to various types of data. The architecture of an ANFIS model typically consists of several layers [17] as follows,

4.1.1. Input Layer

The input layer in an ANFIS is the first component of the architecture and serves as the interface between the input data ((G and T) for the PV system and air pressure (P_a) and fuel pressure (P_f)) and the ANFIS model. Its primary function is to receive the input variables or features and pass them on to the subsequent layers for further processing.

4.1.2. Fuzzification Layer

In the fuzzification layer, each input value is mapped to its degree of membership in the fuzzy sets using fuzzy membership functions. The degree of membership (μ) for an input (x_i) in a fuzzy set (A_i) is calculated using the corresponding membership function (usually Gaussian). The equation for the Gaussian membership function is given as

$$\mu(A_i) = \exp\left(-\frac{(x_i-c_i)^2}{2\sigma i^2}\right) \quad [32]$$

4.1.3. Rule Layer

The rule layer combines the fuzzy membership values from the fuzzification layer to calculate the firing strength of each rule. If you have "m" rules, you will have "m" firing strengths (w_1, w_2, ..., w_m) for each rule, which can be computed using an aggregation operator (usually minimum), which is given as,

$$w_i = \mu(A1_i) \times \mu(A2_i) \times \dots \dots . \mu(An_i) \quad [33]$$

4.1.4. Consequent Layer

The consequent layer represents the consequences of each rule. It consists of single-layer neural networks with parameters that need to be learned. For a regression task, the output of each node in the consequent layer (y_i) can be calculated as a weighted sum of the firing strengths (w_i) with adjustable parameters (θ_i), which is given as,

$$y_i = \emptyset 0_i + \emptyset 1_i \times x_1 + \emptyset 2_i \times x_2 + \cdots . \emptyset n_i \times x_n \quad [34]$$

4.1.5. Output Layer

The output layer combines the outputs from the consequent layer, typically by taking their weighted sum or applying a specific aggregation method. For a single-output ANFIS, it is often a simple sum which is given as,

$$\text{output} = \frac{\in (y_i \times w_i)}{\in w_i} \quad [35]$$

4.1.6. Learning Algorithm

ANFIS uses a learning algorithm to adjust its parameters (θ_i) to minimize a predefined error or loss function. This is typically done using gradient descent or other optimization techniques. The specific equations for parameter updates depend on the chosen optimization method.

ANFIS combines the advantages of two Artificial Intelligence techniques (FLC and ANN) into a single model. An ANFIS works by implementing Artificial Neural Network learning methods to tune the parameters of a Fuzzy Inference System (FIS), and the general architecture of ANFIS is given in Figure 8 [17].

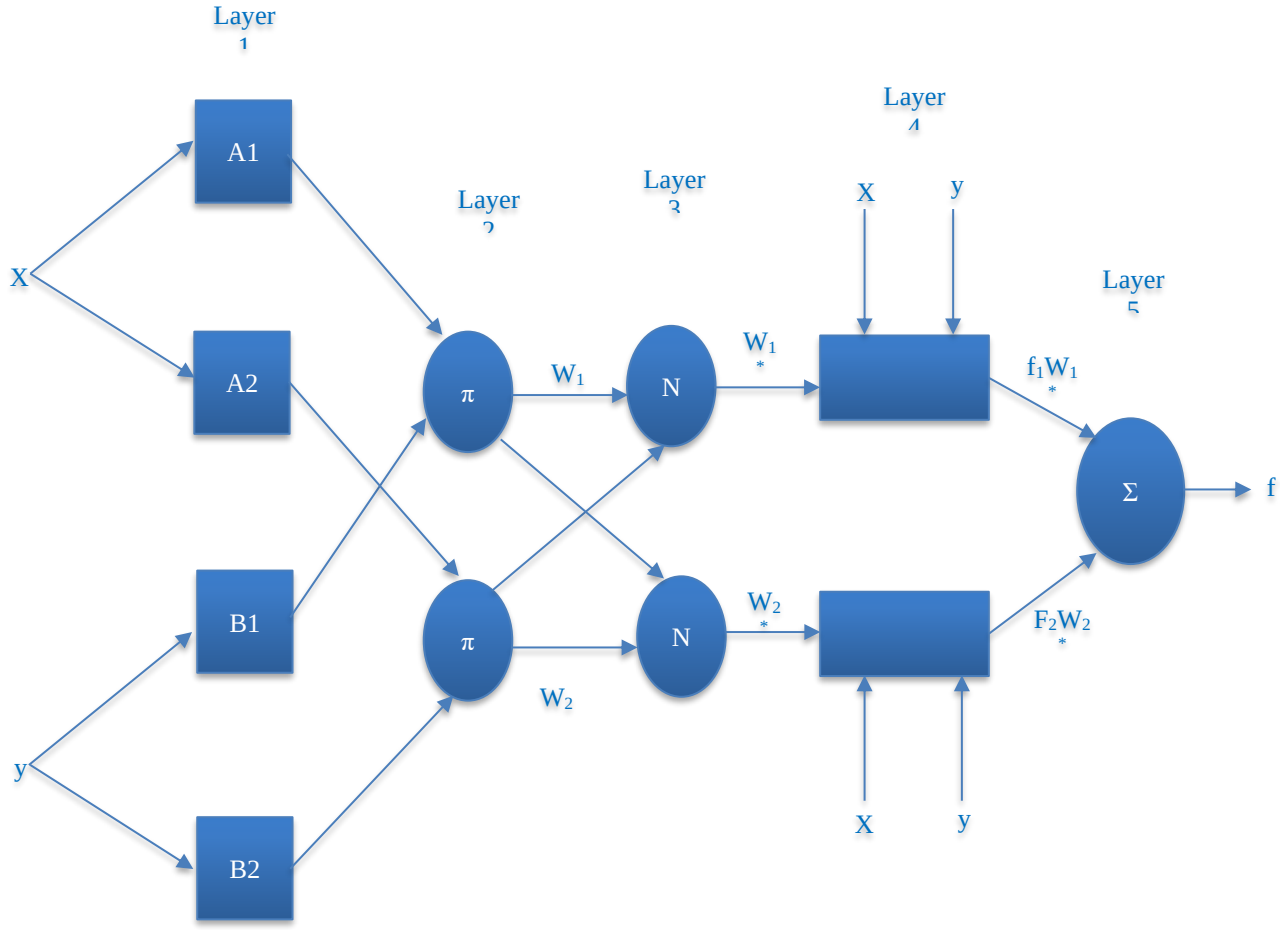

Fig. 8 General ANFIS architecture

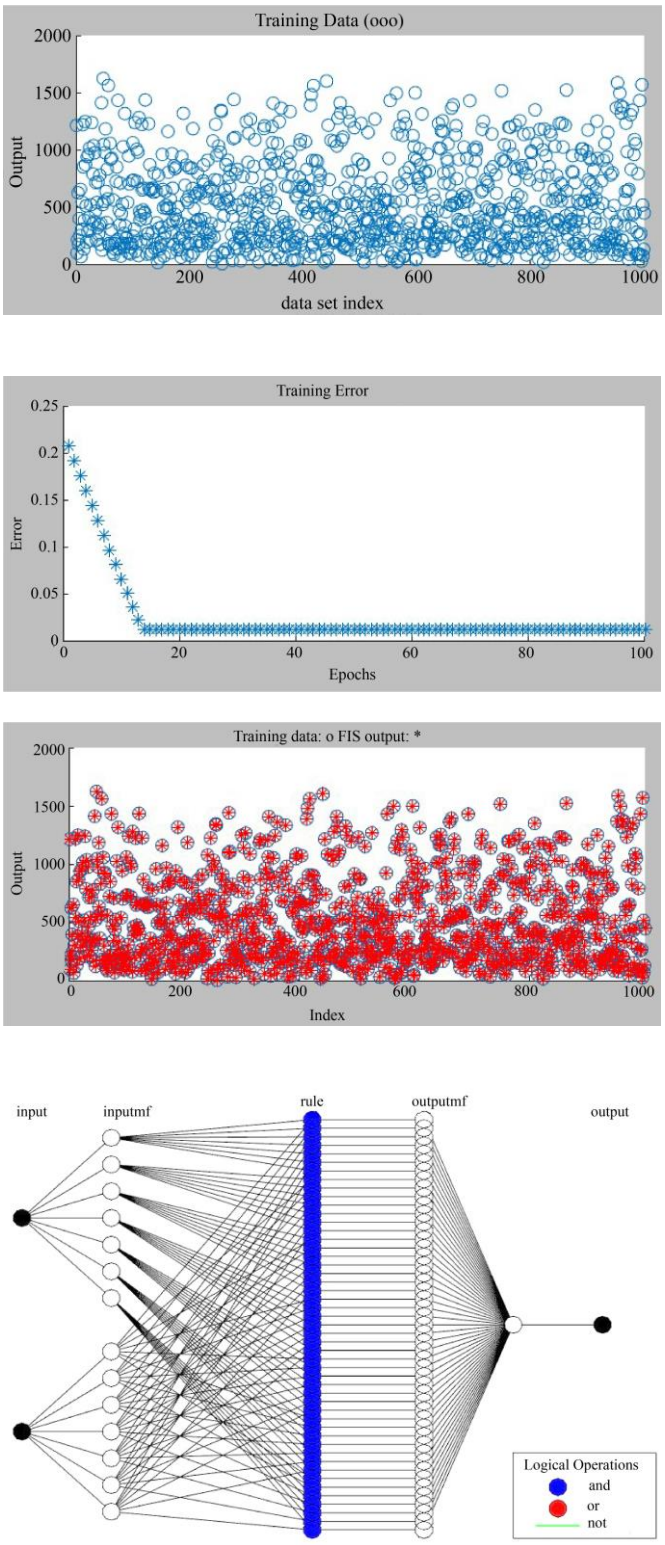

Fig. 9 Process and architecture of ANFIS for PV system

This MPPT control system for the PV system includes the combination of two input data sets (G and T) and output data (P_{max}). These data sets are loaded into the Neuro-fuzzy designer in MATLAB tool, as shown in Figure 9. When using the ANFIS (Adaptive Neuro-Fuzzy Inference System) tool in MATLAB, it is mandated to define the structure and configuration of FIS (Fuzzy Inference System) appropriately. This choice is crucial for achieving accurate MPPT control for the projected photovoltaic system. A 7x7 Membership Functions (MFs) configuration has been implemented in this system, which allows for a more detailed and fine-grained representation of the input variables. This can capture refined shades in the data and potentially result in more accurate modeling. Triangular MFs are selected and it is easy to understand. They have a clear interpretation and are defined by three parameters, namely, the leftmost point, the peak, and the rightmost point. This simplicity makes it easier to design and interpret fuzzy rules for FIS. Linear parameters play a role in the weighted aggregation of fuzzy rule outputs to make a final prediction. The non-linear parameters are typically linked to MFs and determine their shapes and characteristics. The sum of the linear and nonlinear parameters is 91, which represents the overall number of adjustable parameters in the projected ANFIS model. Fuzzy rules are the core of the FIS within ANFIS. Each rule consists of antecedent conditions (if-conditions) and consequent actions (then-actions). These rules describe how input variables are combined to produce output predictions. The presence of 49 fuzzy rules indicates that the projected ANFIS model uses a relatively complex set of rules to capture system behavior. A low RMSE value (0.0132885) indicates that the ANFIS model has achieved a good fit for the training data. It means that the model's predictions are close to the actual training data values.

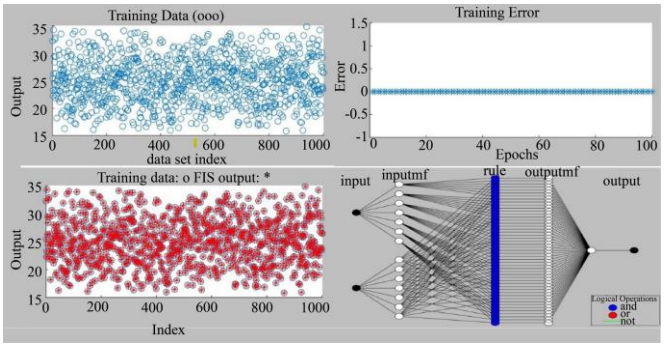

Fig. 10 Process and architecture of ANFIS for PEMFC

This MPPT control system for the PEMFC system includes the combination of two input data sets, air pressure (Pa) and fuel pressure (Pf) and output data (Pmax). These data sets are loaded into the Neuro-fuzzy designer in MATLAB tool, as shown in Figure 10.

4.2. Pi Control

PI control is a classic control algorithm. It will be implemented to regulate the bidirectional DC-DC converter's operation to ensure the battery current and voltage align with the desired reference values. The PI controller begins by measuring the battery current. It then compares this measured current to the desired output current. Finally, it adjusts its

settings to generate a control signal that maintains a consistent output current for the input voltage of the converter changes [18].

5. Performance Analysis of Power Management Across DC Mirco-Grid

The three case studies illustrate different operational scenarios for hybrid renewable energy systems incorporating both PV and PEMFC technologies. Each case presents unique challenges and opportunities in balancing renewable energy generation with power demand requirements are discussed below.

5.1. Case I: Energy Management at Rated PV Power and PEMFC Power with 500W DC Load

At STC, the PV system with ANFIS MPPT generates 1000W with an irradiance of 1000 W/m^2 and a temperature of 25°C, as shown in Figure 11. Similarly, the PEMFC system with ANFIS MPPT generates 1.26KW power with a fuel pressure of 1.5 bar and air pressure of 1 bar at STC, as depicted in Figure 12.

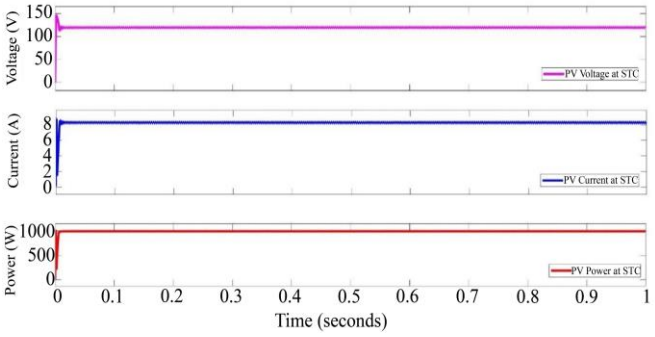

Fig. 11 PV system performance at STC

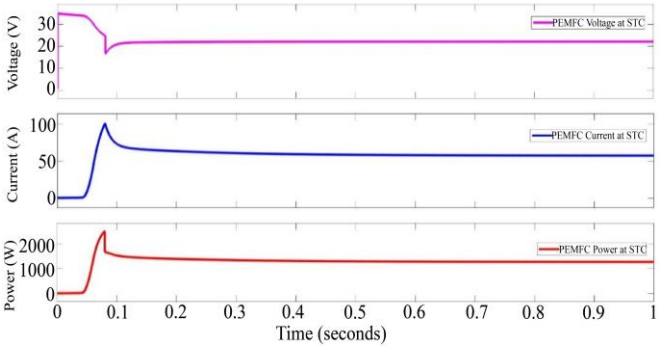

Fig. 12 PEMFC system performance at STC

The total power generated by the PV system and the PEMFC system is utilized to supply the necessary power to the DC load as well as charge the stand-by battery. The DC load constantly consumes 500W, and the remaining power will be utilized for stand-by battery charging, as shown in Figures 13 and 14.

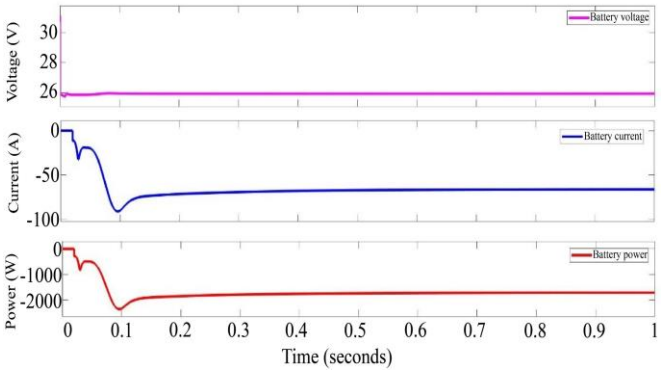

Fig. 13 Stand-by Battery performance at STC

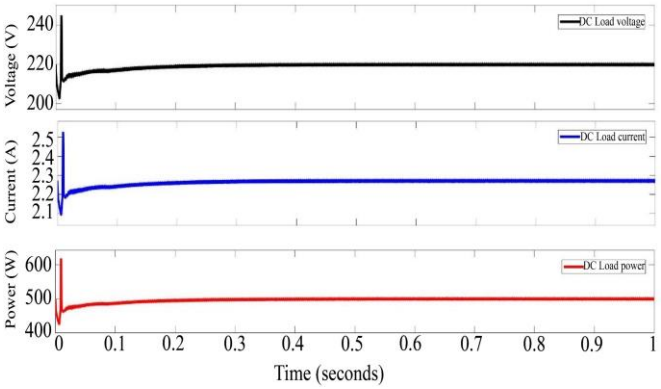

Fig. 14 DC load performance at STC

In Case I, energy management is implemented at rated PV power and PEMFC power under STC. The combined power from both renewable systems is utilized to supply a constant DC load, which is connected through a higher stability SIDC converter, with more surplus power allocated to charging a stand-by battery (SoC=50%).

5.2. Case II: Variable PV Power and Rated PEMFC Power with 500W DC Load

The PV voltage is kept constant by the active ANFIS MPPT controller. The maximum voltage has been harvested from the PV panel always irrespective of changes in irradiance. At dynamic irradiance

($1000W/m^2$ at 0sec,800 W/m^2 at 0.2sec, 500 W/m^2 at 0.5sec & 300 W/m^2 at1sec),

the PV system with ANFIS MPPT generates 1000W initially and gradually decreases along with the variations in irradiance, as depicted in Figure 15. The standby battery charging current is reduced because of the reduction in PV power, as shown in Figure 16. However, the PEMFC system enabled by Artificial intelligence based ANFIS MPPT generates 1.26KW power at STC, and the DC load consumes constant power, as depicted in Figure 17. The active fuel cell system manages the required power for load demand and charging the stand-by battery under the bad performance of the PV system.

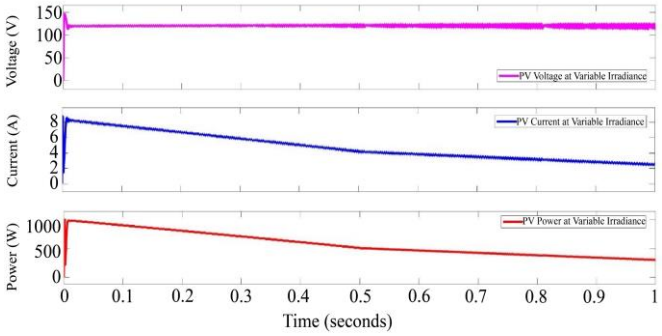

Fig. 15 PV system performance for variable irradiance

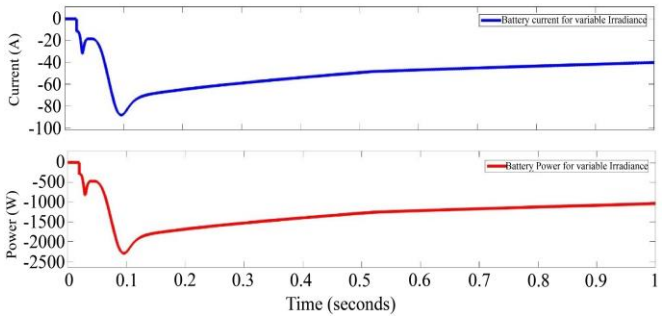

Fig. 16 Battery performance for variable irradiance

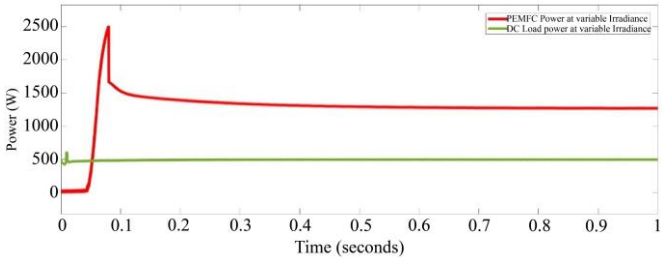

Fig. 17 PEMFC & DC Load performance for variable irradiance

In Case II, effective energy management has been implemented at variable PV power and rated PEMFC power. The combined power from both renewable systems is utilized to supply a constant DC load which is connected through a higher stability SIDC converter, with minimum power allocated to charging a stand-by battery.

5.3. Case III: Rated PV Power and PEMFC Power with 700W DC Load

The PV and PEMFC power is delivered at their maximum values with the increased load power of 700W to investigate the adaptability of the integrated power generation system for variable load. The power management is carried out more accurately and stable, as shown in Figure 18. The power management in PV, PEMFC and BESS-based DC Micro-grid systems with variable DC load has been investigated, and the analysis is depicted in Table 1.

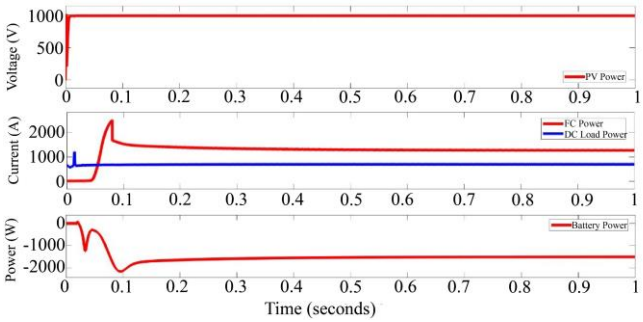

Fig. 18 PEMFC & DC Load performance for variable irradiance

Table 1. Power management strategy

Power Management	Case-I	Case-II	Case-III
PV Power	1000W	1000 to 300W	1000W
PEMFC Power	1260W	1260W	1260W
Stand-by Battery Power	1760W	1760 to 1000W	1560W
DC Load Power	500W	500W	700W

6. Conclusion

This study presents a comprehensive investigation into the efficient power management of a DC microgrid integrating PV, PEMFC and BESS components. Through three distinct operational scenarios, the system's robustness and adaptability are demonstrated by showcasing its capability to balance renewable energy generation with varying load demands. The integration of advanced control algorithms such as ANFIS MPPT and SIDC converters ensures optimized energy conversion and seamless operation. This research contributes valuable insights into the technical intricacies of hybrid renewable energy systems, advancing the development of sustainable microgrid technology.

Acknowledgement

We gratefully acknowledge the support and facilities provided by the authorities of the Annamalai University, Annamalai Nagar, Tamilnadu, India, to carry out this research. We would also like to thank our supporting staff, who gave insight and knowledge that considerably aided the research.

References

[1] Rahmat Khezri, Amin Mahmoudi, and Hirohisa Aki, "Optimal Planning of Solar Photovoltaic and Battery Storage Systems for Grid-Connected Residential Sector: Review, Challenges and New Perspectives," *Renewable and Sustainable Energy Reviews*, vol. 153, 2022. [CrossRef] [Google Scholar] [Publisher Link]

[2] Jiangyan Yan, Jiangyan Yan, and Yajun Wang "A Model of PEMFC-Battery System to Evaluate Inner Operating Status and Energy Consumption Under Different Energy Management Strategies," *International Journal of Hydrogen Energy*, vol. 47, no.5, pp. 3075-3086, 2022. [CrossRef] [Google Scholar] [Publisher Link]

[3] Velamuri Suresh, Nikhil Pachauri, and T. Vigneysh, "Decentralized Control Strategy for Fuel Cell/PV/BESS Based Microgrid Using Modified Fractional Order PI Controller," *International Journal of Hydrogen Energy*, vol. 46, no. 5, pp. 4417-4436, 2021. [CrossRef] [Google Scholar] [Publisher Link]

[4] Suchismita Patel, Arnab Ghosh, and Pravat Kumar Ray, "Efficient Power Management and Control of DC Microgrid with Supercapacitor-Battery Storage Systems," *Journal of Energy Storage*, vol. 73, Part C, 2023. [CrossRef] [Google Scholar] [Publisher Link]

[5] Zheng Nie et al., "Research on Bi-Directional DC / DC Converter for Energy Storage System," *IOP Conference Series: Earth and Environmental Science: 2020 3rd International Conference on Energy and Power Engineering*, Shanghai, China, 2020. [CrossRef] [Google Scholar] [Publisher Link]

[6] Promphak Boonraksa et al., "Design and Simulation of MPPT for PV Systems Using ANFIS Algorithm," *2023 International Electrical Engineering Congress (iEECON)*, Krabi, Thailand, pp. 425-428, 2023. [CrossRef] [Google Scholar] [Publisher Link]

[7] Ramesh Gugulothu, Bhookya Nagu, and Deepak Pullaguram, "Energy Management Strategy for Standalone DC Microgrid System with Photovoltaic/Fuel Cell/Battery Storage," *Journal of Energy Storage*, vol. 57, 2023. [CrossRef] [Google Scholar] [Publisher Link]

[8] Olfa Boubaker, "MPPT Techniques for Photovoltaic Systems: A Systematic Review in Current Trends and Recent Advances in Artificial Intelligence," *Discover Energy*, vol. 3, 2023. [CrossRef] [Google Scholar] [Publisher Link]

[9] Rohit Nandi, Manoj Tripathy, and Chandra Prakash Gupta, "Coordination of BESS and PV System with Bidirectional Power Control Strategy in AC Microgrid," *Sustainable Energy, Grids and Networks*, vol. 34, 2023. [CrossRef] [Google Scholar] [Publisher Link]

[10] Kyeong-Hee Cho et al., "Optimal Sizing Strategy and Economic Analysis of PV-ESS for Demand Side Management," *Journal of Electrical Engineering & Technology*, vol. 19, pp. 2859–2874, 2024. [CrossRef] [Google Scholar] [Publisher Link]

[11] Eleanya Nduka, "Reducing Carbon Footprint by Replacing Generators with Solar PV Systems: A Contingent Valuation Study in Lagos, Nigeria," *Environment and Development Economics*, vol. 28, no. 4, pp. 387–408, 2023.[CrossRef] [Google Scholar] [Publisher Link]

[12] Olga Moraes Toledo, Delly Oliveira Filho, and Antônia Sônia Alves Cardoso Diniz, "Distributed Photovoltaic Generation and Energy Storage Systems: A Review," *Renewable & Sustainable Energy Reviews*, vol. 14, no. 1, pp. 506-511, 2010. [CrossRef] [Google Scholar] [Publisher Link]

[13] Adam Hirsch, Yael Parag, and Josep M. Guerrero, "Microgrids: A Review of Technologies, Key Drivers, and Outstanding Issues," *Renewable and Sustainable Energy Reviews*, vol. 90, pp. 402-411, 2018. [CrossRef] [Google Scholar] [Publisher Link]

[14] Yun Wang et al., "A Review of Polymer Electrolyte Membrane Fuel Cells: Technology, Applications, and Needs on Fundamental Research," *Applied Energy*, vol. 88, no. 4, pp. 981-1007, 2011. [CrossRef] [Google Scholar] [Publisher Link]

[15] Adam Z. Weber, Sivagaminathan Balasubramanian, and Prodip K. Das, "Chapter 2 - Proton Exchange Membrane Fuel Cells," Advances in Chemical Engineering, vol. 41, pp. 65-144, 2012. [CrossRef] [Google Scholar] [Publisher Link]

[16] Eduardo Mg Rodrigues et al., "Comparison of Battery Models for Energy Storage Applications on Insular Grids," *2015 Australasian Universities Power Engineering Conference (AUPEC)*, Wollongong, NSW, Australia, pp. 1-6, 2015. [CrossRef] [Google Scholar] [Publisher Link]

[17] Ahmed Al-Hmouz et al., "Modeling and Simulation of an Adaptive Neuro-Fuzzy Inference System (ANFIS) for Mobile Learning," *IEEE Transactions on Learning Technologies*, vol. 5, no. 3, pp. 226-237, 2012. [CrossRef] [Google Scholar] [Publisher Link]

[18] Remon Das, and Md. Ashraf UddinChowdhury, "PI Controlled Bi-Directional DC-DC Converter (BDDDC) and Highly Efficient Boost Converter for Electric Vehicles," *2016 3rd International Conference on Electrical Engineering and Information Communication Technology (ICEEICT)*, Dhaka, Bangladesh, pp. 1-5, 2016. [CrossRef] [Google Scholar] [Publisher Link]